Available online at www.sciencedirect.com

SciVerse ScienceDirect

Ceramics International 39 (2013) 5855–5862

CERAMICS INTERNATIONAL

www.elsevier.com/locate/ceramint

Characterization of alumino-silicate glass/kaolinite composite

Muthafar F. Al-Hilli*, Kalid T. Al-Rasoul

Department of Physics, College of Sciences, University of Baghdad, Karrada district, Al-Jaderiyah, Baghdad, Iraq

Received 7 July 2012; received in revised form 7 December 2012; accepted 21 December 2012
Available online 17 January 2013

Abstract

A novel porcelain composite of kaolin and alumino-silicate glass (ASG) as a fluxing agent was prepared. The dependence of linear shrinkage, water absorption, apparent porosity and apparent density upon glass addition and sintering temperature were investigated. X-ray diffraction study confirmed the formation of mullite at 1100 °C and existence of cristobalite phase. The glassy phase microstructure was observed using the scanning electron microscope. A self-glazed porcelain body was achieved at 25 wt% of ASG addition. The modulus of rupture (MOR) and flexural strength (σ_f) increased with glass addition, showing maxima values at 15 wt% glass addition. Micro-hardness increased with glass addition and sintering temperature. The dielectric constant (ε'), dielectric loss factor (ε'') and dielectric loss tangent (tan δ) are measured as a function of composition and frequency in the range (10 kHz–1 MHz). The most important property noted was an improvement of the bodies containing ASG in resistance to voltage breakdown. The results of breakdown strength exhibited a maximum value (E_{br} = 56.60 kV/mm) for addition of 25 wt% of alumino-silicate glass sintered at 1100 °C. Owing to its lower cost it is feasible to recycle ASG waste in porcelains instead of feldspar to produce bodies having good properties.

Keywords: Alumino-silicate glass; Kaolinite composite; Dielectrics; Waste recycle

1. Introduction

Ceramic insulators are widely used in microelectronic devices, power transmission as well as distribution lines [1]. The properties required being an insulator is high resistivity, high dielectric strength, a low loss factor, good mechanical properties, dissipation of heat and protection of conductors from severe environment, like humidity and corrosiveness. The glassy phase has the most critical influence on the electrical and mechanical strength of porcelain. In traditional porcelain the main glass-forming component is feldspar or pegmatite [2].

Ceramics are widely used as insulating materials. Ceramic insulators advantages which frequently indicate their use are their superior electrical properties, absence of creep or deformation under stress at room temperature and greater resistance to environmental changes. One of the great advantages of ceramics as insulators is the fact that they are not sensitive to the minor changes in composition, fabrication, techniques, and firing temperature. For the electrical insulation application the properties most concerned are the dielectric and mechanical strength. Dielectric strength (represented by kilovolt per millimeter) measures the ability to withstand large field strength without electrical breakdown. For high-tension electrical insulation the dielectric strength has to be above (30 kV/mm) [3].

In the European Union states for example, annually more than 2 million tons of industrial wastes including metallurgical slag and waste glass are deposited. They contain a high concentration of toxic substances, heavy metals, organic substances, soluble salts etc. Technologies for materials wastes recycling are being developed for environmental protection against toxic pollution. Simultaneously, technologies that aim at their secondary processing into new inert materials of high quality and low energy and time consumption are also developed. Recycling is one of the most important processes for glass waste reprocessing. The percentage of glass recycling varies in dependence of its

*Corresponding author.
E-mail addresses: mfj972@yahoo.com, m.alhilli@scbaghdad.edu.iq (M.F. Al-Hilli).

0272-8842/$ - see front matter © 2013 Elsevier Ltd and Techna Group S.r.l. All rights reserved.
http://dx.doi.org/10.1016/j.ceramint.2012.12.102

color: 82%-green, 44.5%-brown and 43.8%-white glass. The glass waste are used as raw materials for obtaining of new materials and composites with possibilities for various applications in the environmental protection, as compact and porous glass-ceramics materials, Portland cement, fillers, catalysts, pigments, porcelain, filters, dust collectors, decorative and construction covers and barriers [4]. Alumino-silicate glass is frequently used in semiconductor and optical industry and to control release of volatile chemicals. It is widely used in micro-electro mechanical system (MEMS) due to its good durability, smoothness, high electrical properties and high optical transparency [5]. Porcelain is a white, non-porous and partially transparent ceramic material of traditional composition (silica, feldspar and kaolin). The kaolin group of minerals with example of ideal formulas for kaolinite $Al_2(OH)_4 \cdot Si_2O_5$ and halloysite $Al_2(OH)_4 \cdot Si_2O_5 \cdot 2H_2O$. While the feldspar acts as the fluxing material in the porcelain mixture [6].

However very little information is available in literatures about the substitution of feldspar in electrical porcelain. Some researcher have investigated the use of Ornamental Rock Waste in electrical Porcelain by Silva and Holanda [7], recycling of scrape in porcelain stoneware by Karamanov et al. [8], use of glass waste in porcelain stoneware tile mixtures by Luz and Ribeiro [9]. This work is part of a more extensive investigation to study the effect of feldspar substitution by different fluxing agents on the high tension insulators properties. With this aim, the present study covers the replacement by alumino-silicate glass (ASG) of the feldspar in a high tension electrical porcelain preparation. The work discusses the possibility of glass waste recycling in the production of electric porcelain sintered at low temperature. The prepared insulators were evaluated according to its physical, mechanical, dielectric and electrical properties.

2. Experimental

The kaolin and alumino-silicate glass (ASG) powders were sieved through (63 μm) screen. The ASG powder was added to kaolin in proportions of (5, 10, 15, 20 and 25% wt%), and dry mixed using a ball mill. Sample pellets were prepared by uniaxial semi-dry pressing using a pressure of 374.3 MPa. The samples were dried over night at ambient, and then the final sintering was carried out at different temperatures. The sintering process carried out in air with heating rate of 3 °C/min and soaking period 1/2 h using Carbolite muffle furnace. Then the samples were left to cool down to room temperature naturally. The X-ray diffraction characterization was performed on xrd Shimadzu 6000 with CuKα radiation ($\lambda = 1.540598$ Å). The samples linear shrinkage (L.S%) is determined by measuring the samples dimensions before and after sintering.

$$\text{L.S\%} = \frac{\text{dry length} - \text{fired length}}{\text{dry length}} \times 100\% \quad (1)$$

The water absorption percentage was determined from Eq. (2) using the vacuum/boiling technique [10,11]. The samples were weighed immediately after sintering to find dry weight (W_D). The samples were soaked in distilled water and contained in suitably protected desiccators for 2.5 h at pressure of 25 mbar. Afterwards, the samples were left in gently boiling water for 1 h and soaked for an additional 24 h at ambient temperature. The samples were taken and wiped with moistened tissue and weighed to find the soaked weight (W_S). To find the immersed weight (W_I), the sample suspended from the arm of a balance pan and immersed in distilled water. The apparent porosity (A.P%) and apparent density (A.D) are determined from Eqs. (3) and (4), respectively. The measurements were carried out according to Archimedes principle [ASTM test method (20–83, 493–70)].

$$\text{W.A\%} = \frac{W_S - W_D}{W_D} \times 100\% \quad (2)$$

$$\text{A.P\%} = \frac{W_S - W_D}{W_S - W_I} \times 100\% \quad (3)$$

$$\text{A.D} = \frac{W_D}{W_D - W_I} \quad (4)$$

where L.S% is the linear shrinkage percent, W.A% is the water absorption percent, A.P% is the apparent porosity percent and A.D is the apparent density (g/cm^3). The surface morphology was characterized by a scanning electron microscope instrument JEOL JSM-6400.

The modulus of rupture (MOR) measurement was performed on the INSTRON model 1122 instrument. The test was carried out using three-bearing cylinders mechanism mounted between the platens of the testing device. The crosshead speed was (0.5 mm/min) with maximum load of (2000 N). Rectangular shaped samples of dimensions ($5 \times 5 \times 22$ mm^3) sintered at 1100 °C were broken over (17 mm) span. Only the results of the specimens broken at mid span were taken into account. The maximum load of fracture was recorded and modulus of rupture (MOR) was obtained as follows:

$$\text{MOR} = \frac{3FS}{2bt^2} \quad (5)$$

where F is the load at failure (N), S is the distance between supports (span), b is the sample breadth and t is the sample height [12]. The flexural strength (σ_f) was measured by the diametrical compression test of a solid disk specimen referred to as the Brazilian disk fracture test. The test performed on a disk specimen (height = 5 mm × diameter = 13 mm) performed on the INSTRON model 1122 instrument. The specimen was fixed between the device platens to start compressing at a crosshead speed = 0.5 mm/min until fracture occurred. The flexural strength (diametrical compression strength) is determined from the relationship

$$\sigma_f = \frac{2F_{\text{fract.}}}{\pi Dh} \quad (6)$$

where ($F_{fract.}$) is the fracture load (N), (D) is the sample diameter and (h) is the sample thickness [13,14]. The Vickers indentation test is a common method used to characterize the hardness of materials. These experiments are simple to perform, need a small quantity of material, are generally non-destructive and can be repeated many times. Vicker's micro-hardness instrument HPO250 equipped with microscopic screen and diagonal measuring device was used to measure the hardness. The samples were grinded and polished to mirror-like surface and coated with an aluminum thin coating ≈ 00 Å to ensure a clear evident indent on the sample surface. The optimum indentation load was (49 N) for loading time of (15 s). Three indents were made on each sample surface. The average of indent diagonals dimensions was taken to determine the Vicker's hardness (H_V)

$$H_V = 1.8544\left(\frac{F_a}{d^2}\right) \quad (7)$$

where F_a is the applied indenter load (N) and d is the average diagonal length for the indent (mm) [15,16].

The dielectric constant (ε'), dielectric loss factor (ε'') and dielectric loss tangent ($\tan\delta$) were measured using a Precision LCR Meter, model HP 4284A/1988. Samples of thickness = 2 mm and diameter = 20 mm were used for this test. The samples were coated on both sides with an aluminum thin film layer to make capacitor of the samples.

The breakdown strength was performed on "High Voltage Potronics Device" at 50 Hz with maximum negative voltage of 80 kV. Pure transformer oil with breakdown strength about 40 kV/mm was used as the testing ambient medium to prevent the surface breakdown or flash-over voltage. The voltage was raised at a rate of 1 kV/s to ensure eliminations of any thermal effects until breakdown occurred at the maximum breakdown voltage (V_{br}) to determine the breakdown strength (E_{br})

$$E_{br} = \frac{V_{br}}{h} \quad (8)$$

where h is the sample thickness in (mm).

3. Results and discussion

The chemical analyses of the kaolin and alumino-silicate glass are given in Tables 1 and 2, respectively. Quartz addition was eliminated in the present study to focus on the effect of glass addition on the properties of kaolin bodies. However, the high percentage of quartz in both kaolin and alumino-silicate glass compensated the absence of quartz in the prepared porcelain.

The X-ray diffraction pattern of the sample with 25% ASG addition is shown in Fig. 1. Kaolinite group clays undergo a series of phase transformations upon thermal treatment in air at atmospheric pressure. Endothermic dehydroxylation begins at 550–600 °C to produce disordered metakaolin $Al_2Si_2O_7$. Farther heating to 900 °C converts metakaolin to an aluminum–silicon spinel, $Si_3Al_4O_{12}$ which is sometimes also referred to as a gamma-alumina type structure

$$2Al_2Si_2O_7 \rightarrow Si_3Al_6O_{13} + 5SiO_2$$

Upon calcination to 1050 °C, the spinel phase nucleates and transforms to mullite and highly crystalline cristobalite, SiO_2

$$3Si_3Al_4O_{12} \rightarrow 2Si_2Al_6O_{13} + SiO_2$$

At such temperature the mixture will contain crystobalie and quartz (this comes as impurities in natural clay). Mullite formation was detected with the sample containing 25% ASG sintered at 1100 °C, whereas the transformation of β-quartz to β-cristobalite does not take place, in agreement with Márquez et al. [17,18].

The results of linear shrinkage (L.S)%, water absorption (W.A)%, apparent porosity (A.P) % and apparent density (A.D) are given in Table 3. Linear shrinkage increased with sintering temperature and ASG wt%, since the body becomes richer with molten glass. The molten glass helps to fill up the inter-particles spacing as a result of which sample volume was reduced. Water absorption and apparent porosity, which are correlated to each other, were found to decrease with both of sintering temperature and ASG wt%. Since water absorption and porosity which reflected the degree of vitrification were, in general, controlled by the type and content of fluxing mineral. Water absorption must not exceeds (0.5%) for the high voltage electrical porcelain. The water absorption and

Table 1
Chemical analysis of kaolin.

Oxide	SiO_2	Al_2O_3	Fe_2O_3	TiO_2	CaO	MgO	Na_2O	K_2O	L.O.I.
%	47.34	36.37	0.63	2.20	0.02	0.08	0.31	0.53	12.42

Table 2
Chemical analysis of alumino-silicate glass (ASG).

Oxide	SiO_2	Al_2O_3	B_2O_3	MgO	CaO	BaO
%	57	16	4	7	10	6

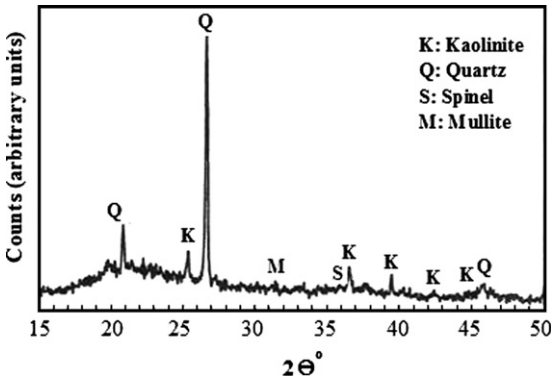

Fig. 1. X-ray diffractogram of porcelain body fired at 1100 °C. K, kaolinite; Q, quartz; S, spinel and M, mullite.

Table 3
Change in linear shrinkage (L.S%), Water absorption (W.A%), Apparent porosity (A.P%) and Apparent density (A.D g/cm^3) with sintering temperature and ASG wt%.

	Sintering temperature (°C)																			
	800					**900**					**1000**					**1100**				
ASG wt%	**5**	**10**	**15**	**20**	**25**	**5**	**10**	**15**	**20**	**25**	**5**	**10**	**15**	**20**	**25**	**5**	**10**	**15**	**20**	**25**
L.S %	6.5	6.0	5.5	5.3	5.1	8.7	9.3	9.4	10.0	10.2	10.1	10.2	10.5	11.0	13.0	14.6	14.8	14.9	16.8	16.9
W.A %	16.7	15.5	15.0	16.6	17.8	13.1	10.0	10.6	10.9	10.0	11.2	9.7	7.7	6.5	5.4	5.3	4.8	2.5	0.2	0.0
A.P %	28.5	21.5	26.0	27.0	27.5	24.8	19.9	21.5	22.0	20.0	23.0	20.5	16.4	15.3	13.0	12.6	12.0	6.0	0.15	0.0
A.D (g/cm^3)	2.39	2.27	2.23	2.18	2.15	2.46	2.47	2.57	2.52	2.49	2.66	2.67	2.68	2.65	2.63	2.73	2.65	2.60	2.54	2.51

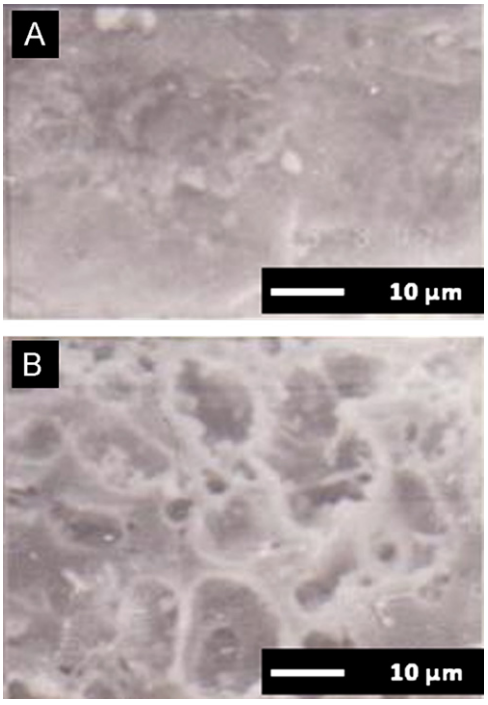

Fig. 2. SEM micrograph of the sample contains 15 wt% of ASG sintered at 1100 °C. (A) glassy phase fill up pore on the surface and (B) undissolved cristobalite crystals.

apparent porosity dropped to zero upon addition (ASG wt% = 25) for the sample sintered at 1100 °C. The apparent density increased with sintering temperature, and reached maximum density = 2.73 g/cm^3 for the sample with 5 wt% of ASG addition sintered at 1100 °C. According to the models of sintering by viscous flow of glass, such as Frenkel's and Mackenzie-Shuttleworth's models, the sintering rate depends directly on the surface tension and inversely on the viscosity of the liquid phase at the firing temperature [19]. When there is a suitable amount of glassy phase content it is quite advantageous to the ceramic insulator as it only fills up the pores as shown in Fig. 2A. Some residual undissolved cristobalite crystals were seen in Fig. 2B, which increased the mechanical strength by hindering crack propagation.

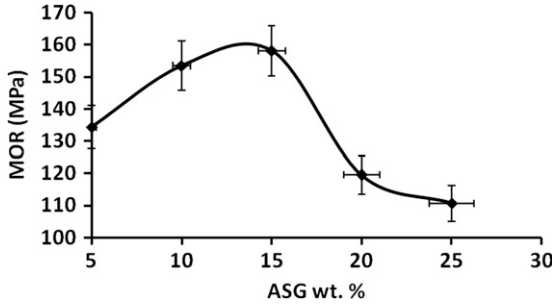

Fig. 3. Modulus of Rupture (MOR) versus ASG wt%, for the sample sintered at 1100 °C.

Fig. 3 shows the dependence of modulus of rupture (MOR) upon the addition of ASG wt%. The maximum value of the MOR was observed at 15 wt% of ASG addition due to the decrease in porosity. The decrease in MOR for the ASG addition > 15%, may be attributed to the decrease in density from (2.60 g/cm^3) to (2.51 g/cm^3). In addition, the porcelain body becomes very rich with the glassy phase which is mechanically a weak phase. To increase fracture toughness or specific fracture energy of ceramics generally involve manipulation and tailoring of the microstructure. The microstructure can be improved by optimizing the proportions of the individual phases, including crystalline and glassy phases. If the ceramic body contains a relatively high proportion of glassy phase, the crack will primarily propagate through this phase and the properties of the other phases will have little effect as illustrated in Fig. 4.

Fig. 5 shows the diametrical compression strength (σ_f) as a function of ASG addition. The diametrical compression strength behavior versus ASG addition was found to agree with that of the MOR. However, the diametrical compression strength showed lower values than those of the MOR, due to the difference in stresses distribution. This shows that the relationship between the two tests is not straightforward in agreement with the postulate of Vardar and Finnie [13]. The dependence of flexural strength on the sintering temperature is given in Table 4. The flexural strength increased with sintering temperature. This increase of flexural strength with sintering temperature

may be related to the mullite crystallization at sintering temperature 1100 °C as shown in Fig. 6. A significant part was also played by the sintering process and the presence of pores. Residual pores were then removed after sintering through glass infusion. As far as pores are concerned, these should not arise at grain boundaries where they increase the stress concentration at points where weakened bonds already occur. In contrast to this, pores of spherical shape arising for example in the glassy phase may even have a favorable effect by blunting the crack front so that greater energy is required for its growth. Fracture energy is related to the energy consumed during crack propagation. This energy consumption is due to the presence of barriers that increase the crack path until the complete fracture of the sample. The presence of a higher content of crystalline phases, mainly quartz, primary and secondary mullite and higher density means higher strength of the samples [20]. Another factor that may play a significant role is the aspect ratio of mullite needles, which start formation at 1100 °C and grew inside the pores, leading to a strengthening of the porcelain body [21].

Vicker's micro-hardness was observed to increase with sintering temperature and ASG content as shown in Table 4 and Fig. 7, respectively. The micro-hardness increase is attributed to the surface self-glazing by the molten glassy phase. Moreover, the hardness increase with sintering temperature may be related to the stimulated formation of mullite crystals at sintering temperature 1100 °C (mullite hardness ≈ 15 GPa) [22,23]. It may be concluded that the addition of glass powder had a positive effect on the mechanical properties and that the variation of the properties was mainly related to the vitrification and residual porosity. These results agree with the observations of Karamanov et al. [8].

The components of polarizability are $\alpha_e+\alpha_i+\alpha_o+\alpha_s$ representing susceptibilities associated with electronic, ionic, orientation, and space charge polarization, respectively. The electronic polarization is due to shifts or displacement of electron clouds in the dielectric field away from their equilibrium positions, resulting in a net dipolar response. It occurs in all solids up to optical frequencies $\sim 10^{16}$ Hz. Ionic polarization results from similar ionic displacement in the field and occurs up to the infrared region of 10^{10}–10^{13} Hz. In contrast, orientation polarization is both frequency (time) dependent and temperature dependent, since it represents dipole orientation and ion jump polarization. The remaining process, the space charge or interfacial polarization, is produced by traveling charge carriers. However, they exhibit different frequency responses and can be separated. At low frequencies, all four sources of polarization are important, whereas at

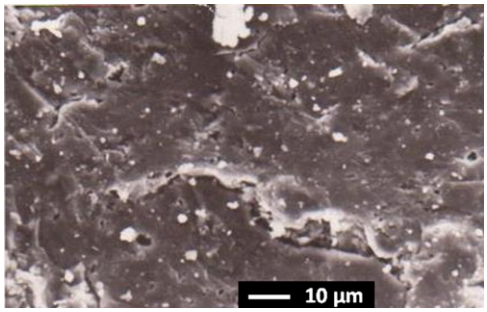

Fig. 4. SEM micrograph shows crack propagation in porcelain sample contains 15 wt% of ASG sintered at 1100 °C.

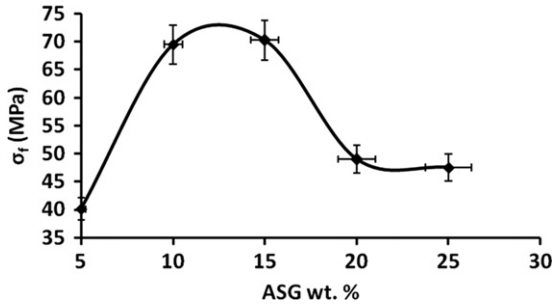

Fig. 5. Flexural strength (σ_f) versus ASG wt%, for the sample sintered at 1100 °C.

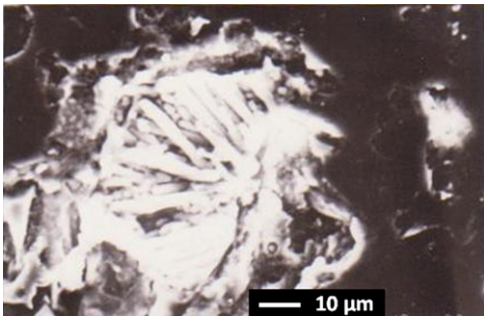

Fig. 6. SEM micrograph shows the mullite needle-like crystals of the sample contains 25 wt% of ASG sintered at 1100 °C.

Table 4
The dependence of Vicker's hardness (H_V) and flexural strength (σ_f) on the sintering temperature for the sample composition (kaolin+15 wt. % aluminosilicate glass).

Sintering temperature (°C)	Vicker's hardness, H_V (GPa)	Flexural strength, σ_f (MPa)
800	0.6	9.3
900	0.8	12.1
1000	1.4	26.4
1100	4.6	71.8

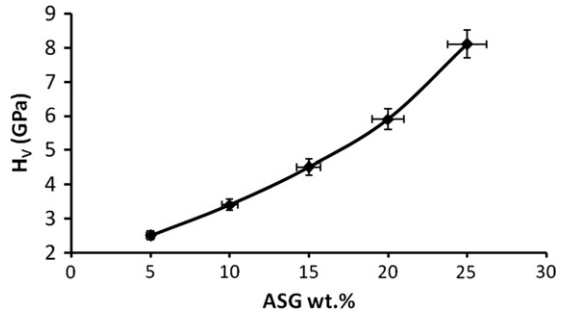

Fig. 7. Vicker's micro-hardness (H_V) versus ASG wt%, for the sample sintered at 1100 °C.

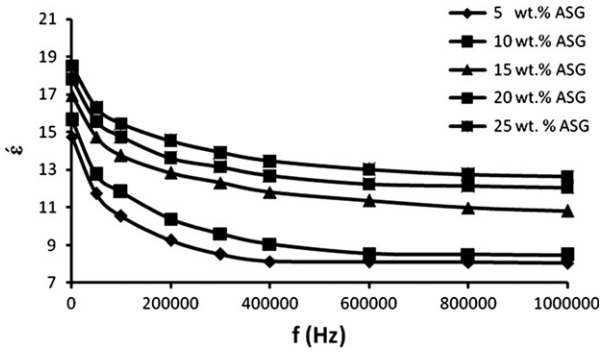

Fig. 8. Dielectric constant (ε') versus frequency (f) for kaolin+ASG, for the sample sintered at 1100 °C.

optical frequencies, i.e., above optical phonon frequencies, only the electronic polarization comes into play. In the absence of dipolar polarization, permittivity should be non-dispersive for frequencies up to microwave frequencies. Thus, dispersion below microwave frequencies results from dipolar polarization effects and space charge or interfacial polarization (Maxwell–Wagner relaxation polarization). Therefore, they play a main role in our dielectric measurement. The dielectric constant (ε') as a function of frequency and alumino-silicate glass addition is plotted in Fig. 8. The dielectric permittivity is a complex number composed of real and imaginary parts. The real part results from the polarization of material, whereas the imaginary part is related to Ohmic and polarization losses [24]. The dielectric constant was noticed to increase with ASG addition owing to the increase in interfacial Maxwell–Wagner relaxation polarization in agreement with Koop's phenomenological theory. The dielectric constant was observed to decrease rapidly in the frequencies range (10^3–10^5 Hz), as the space charge polarizability is damped out. Then the decrease in the dielectric constant became more stable with frequency increase up to (10^6 Hz), where the dipolar polarizability was suppressed.

The dependence of dielectric loss factor (ε'') and dielectric loss tangent ($\tan\delta$) on the frequency (f) is shown in Fig. 9 and Table 5, respectively. The dielectric loss was found to decrease with the ASG addition. The eddy current loss mainly depends on the electrical resistivity of the porcelain. So, it may be considered that the lowering of

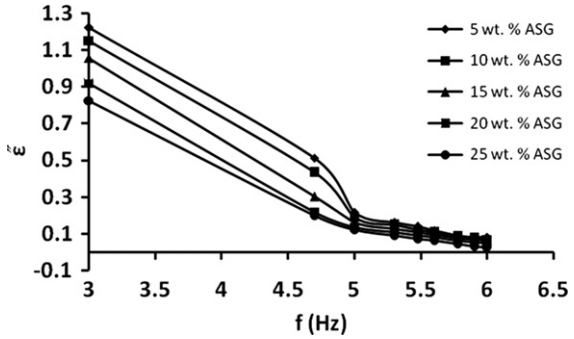

Fig. 9. Dielectric loss factor (ε'') versus frequency (f) for kaolin+ASG, for the sample sintered at 1100 °C.

Table 5
The dependence of tangent dielectric loss angle ($\tan\delta$) on the frequency (f) and addition of ASG wt% for the samples sintered at 1100 °C.

tan δ					
***f* (kHz)**	**ASG (wt%)**				
	5	**10**	**15**	**20**	**25**
10	0.0827	0.0735	0.0621	0.0514	0.0445
50	0.0435	0.0339	0.0204	0.014	0.0122
100	0.0206	0.0158	0.0117	0.0091	0.0079
200	0.0175	0.014	0.0099	0.0078	0.0062
300	0.0162	0.0127	0.0086	0.0068	0.0052
400	0.0143	0.0116	0.0078	0.0062	0.0045
600	0.0111	0.0096	0.0065	0.0049	0.0033

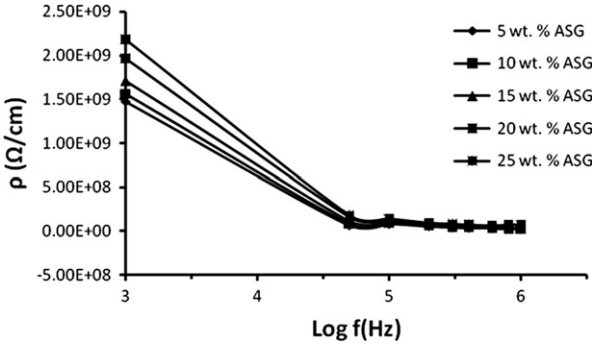

Fig. 10. AC resistivity versus frequency (f) for kaolin+ASG, for the sample sintered at 1100 °C.

dielectric loss in porcelain results mainly from a reduction in eddy current loss due to their higher electrical resistivity. The decrease in (ε'') with increasing frequency agrees well with Deby's type relaxation process [25]. Fig. 10 shows the AC resistivity as a function of frequency for different ASG addition levels. The resistivity (ρ) was determined from the relation

$$\rho = \frac{1}{\omega\,\varepsilon_o\varepsilon''} = \frac{1}{\omega\,\varepsilon_o\varepsilon'\tan\delta} \tag{9}$$

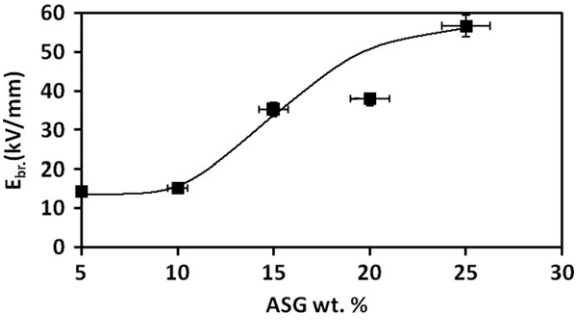

Fig. 11. Dielectric breakdown strength (E_{br}) versus ASG wt%, for the sample sintered at 1100 °C.

where ε_o is the vacuum permittivity, ε' is the dielectric constant, ε'' is the dielectric loss factor and $\tan\delta$ is the tangent of dielectric loss angle [26]. The decrease in resistivity with frequency can be explained by Koop's theorem, which supposed that the ceramic compact acts as a multilayer capacitor. In this model, the porcelain grain and grain boundaries have different properties. The effect of the multilayer capacitor increases with frequency; as a result the resistivity decreases [27]. The resistivity increased with glass addition due to the decrease in porosity.

The dielectric breakdown strength dependence on the alumino-silicate glass addition is shown in Fig. 11. The breakdown strength was found to increase with the glass addition mainly due to the porosity decrease. This behavior agrees well with the widely accepted Gerson-Marshall Model related to effects of porosity on breakdown strength of porous ceramics. According to the Gerson-Marshall model, the measured dielectric strength in porous ceramics depends on the porosity and pore size [28]. The dominant mechanism of breakdown in the high voltage porcelain insulators is, a small number of carriers in the conduction band are accelerated in the electric field and these collide with atoms, ionizing them. This releases more carriers for further impact ionization and the current rapidly builds. However, the resultant Joule heating causes insulators to become better conductors that can pass more current. The process feeds on itself until a thermal runaway result in local failure of the insulator. Shaping the insulators in special ways can effectively reduce their tendency to breakdown or conduct at high voltages.

4. Conclusion

In conclusion, glass powder waste showed to be an efficient fluxing agent when it was used as an additive in porcelain mixture. During sintering process, glass waste powder accelerated the densification process and decreased the sintering temperature and sintering time interval. The low sintering temperature 1100 °C and short sintering interval (1/2 h) reduced the energy consumption in the preparation of the insulators. Except the disadvantage of linear shrinkage increase, the water absorption, apparent porosity and density were improved by and self-glazing body due to addition of ASG to kaolin. The ASG addition was responsible for the mechanical and electrical properties improvement in the prepared high voltage insulator. The improvements in mechanical properties were mainly related to the residual porosity. The difference between diametrical compression strength and MOR was attributed to the difference in stresses distribution. The low dielectric constant provides the advantage of using the insulator in high speed electronic circuits (capacitor dielectrics). The prepared insulators showed low dielectric losses due to the reduction in eddy current losses. The breakdown strength was increased by decreasing the porosity with the glass addition. The use of ASG waste in the preparation of high voltage insulators should reduce production costs which makes its utilization very attractive. Nevertheless, the obtained material is suitable for industrial exploitation because of its high properties (mechanical, electrical and dielectric strength).

References

[1] A. Roula, K. Boudeghdegh, N. Boufafa, Improving usual and dielectric properties of ceramic high voltage insulators, Cerâmica 55 (2009) 206–208.
[2] K.N. Gorbunova, G.V. Dudinova, I.S. Stefanenko, Using perlite to produce low-voltage electrical porcelain, Glass and Ceramics 40 (6) (1984) 305–307 (Translated from Steklo i Keramika, No. 6, June (1983) 20–21).
[3] Rashed Adnan Islam, Y.C. Chana, Md. Fakhrul Islam, Structure–property relationship in high-tension ceramic insulator fired at high temperature, Materials Science and Engineering B 106 (2004) 132–140.
[4] V. Vassilev, E. Fidancevska, M. Milosevski, S. Parvanov, D. Milosevski, T. Hristova-Vasileva, Composites based on industrial wastes IV. Production of porous composites from Fe–Ni slag and waste, Journal of the University of Chemical Technology and Metallurgy 42 (4) (2007) 369–376.
[5] H.T. Ting, K.A. Abou-El-Hossein, H.B. Chua, Prediction of etching rate of alumino-silicate glass by RSM and ANN, Journal of Scientific and Industrial Research 68 (2009) 920–924.
[6] Apinon Nuntiya, Sitthisak Prasanphan, The rheological behavior of kaolin suspensions, Chiang Mai Journal of Science 33 (3) (2006) 271–281.
[7] M.A. Silva, J.N.F. Holanda, Electrical porcelain containing, ornamental rock waste: microstructural development, Materials Science Forum 660-661 (2010) 692–696.
[8] Alexander Karamanov, Emilia Karamanova, Anna Maria Ferrari, Fabiola Ferrante, Mario Pelino, The effect of fired scrap addition on the sintering behaviour of hard porcelain, Ceramics International 32 (2006) 727–732.
[9] A.P. Luz, S. Ribeiro, Use of glass waste as a raw material in porcelain stoneware tile mixtures, Ceramics International 33 (2007) 761–765.
[10] W. Ryan, C. Radford, White Wares: Production Testing and Quality, Control pergamon press, UK, 1987.
[11] J. Martín-Márquez, J. Ma., Rincón, M. Romero, Effect of firing temperature on sintering of porcelain, stoneware tiles, Ceramics International 34 (2008) 1867–1873.
[12] Vanessa Vásquez, Mutlu Özcan, Renato Nishioka, Rodrigo Souza, Alfredo Mesquita, Carlos Pavanelli, Mechanical and thermal cycling effects on the flexural strength of glass ceramics fused to titanium, Dental Materials Journal 27 (1) (2008) 7–15.
[13] O. Vadar, I. Finnie, An analysis of the brazilian disk fracture test using the weibull probabilistic treatment of brittle strength, International Journal of Fracture 11 (3) (1975) 495–508.

[14] D.M. Williamson, S.J.P. Palmer, W.G. Proud, R. Govier, Brazilian disc testing of a UK PBX approaching the glass transition condition, shock compression of condensed matter, in: Proceedings of the American Physical Society Topical Group on Shock Compression of Condensed Matter, vol. 1195, 2009 pp. 494–497.
[15] W.P. Herman, Materials Science and Metallurgy, 3rd edition, Reston Pub. Co., Virginia, 1981.
[16] D. Quim, Parimal J. Patel, Isabel Lloyd, Effect of loading rate upon conventional ceramic hardness, Journal of Research of the National Institute of Standards and Technology 107 (3) (2002) 299–306.
[17] Jorge Martn-Márquez, Angeles G. De la Torre, Miguel A.G. Aranda, Jesús Ma Rincón, Maximina Romero, Evolution with temperature of crystalline and amorphous phases in porcelain stoneware, Journal of the American Ceramic Society 92 (1) (2009) 229–234.
[18] Jorge Martn-Márquez, Jesús Ma Rincón, Maximina Romero, Mullite development on firing in porcelain stoneware bodies, Journal of the European Ceramic Society 30 (2010) 1599–1607.
[19] C. Zanelli, G. Baldi, M. Dondi, G. Ercolani, G. Guarini, M. Raimondo, Glass ceramic frits for porcelain stoneware bodies: effects on sintering, phase composition and technological properties, Ceramics International 34 (2008) 455–465.
[20] Saulo Roco Bragaça, Carlos Pérez Bergmann, Waste glass in porcelain, Materials Research 8 (1) (2005) 39–44.
[21] Jorge Martn-Márquez, Jesús Ma Rincón, Maximina Romero, Effect of microstructure on mechanical properties of porcelain stoneware, Journal of the European Ceramic Society 30 (2010) 3063–3069.
[22] Dragan Leposava Sidjanin, Jonjaua Rajnovica, Ranogajec, Elvira Molnar, Measurement of Vickers hardness on ceramic floor tiles, Journal of the European Ceramic Society 27 (2007) 1767–1773.
[23] Parvati Ramaswamy, S. Vynatheya, S. Seetharamu, Significance of structure–property relationship in alumina based porcelain insulators to achieve quality, Bulletin of Materials Science 28 (7) (2005) 681–688.
[24] Abidin Kaya, Electrical spectroscopy of kaolin and bentonite slurries, Turkish Journal of Engineering and Environmental Sciences 25 (2001) 345–354.
[25] E. Ateia, M.A. Ahmed, A.K. El-Aziz, Effect of rare earth radius and concentration on the structural and transport properties of doped Mn–Zn ferrite, Journal of Magnetism and Magnetic Materials 311 (2007) 545–554.
[26] M.A. Ahmed, E. Ateia, S.I. El-Dek, Rare earth doping effect on the structural and electrical properties of Mg–Ti ferrite, Materials Letters 57 (2003) 4256–4266.
[27] S.A. Mazen, Infrared absorption and dielectric properties of Li–Cu ferrite, Materials Chemistry and Physics 62 (2000) 139–147.
[28] Oratai Jongprateep, Vladimir Petrovsky, Fatih Dogan, Effects of yttria concentration and microstructure on electric breakdown of yttria stabilized zirconia, Journal of Metals, Materials and Minerals 18 (1) (2008) 9–14.